J|A|C|S ARTICLES

Published on Web 03/10/2010

Molecular-Mechanical Switching at the Nanoparticle−Solvent Interface: Practice and Theory

Ali Coskun, Paul J. Wesson, Rafal Klajn, Ali Trabolsi, Lei Fang, Mark A. Olson, Sanjeev K. Dey, Bartosz A. Grzybowski,* and J. Fraser Stoddart*

Department of Chemical and Biological Engineering and Department of Chemistry, Northwestern University, 2145 Sheridan Road, Evanston, Illinois 60208-3113

Received December 3, 2009; E-mail: grzybor@northwestern.edu; stoddart@northwestern.edu

Abstract: A range (Au, Pt, Pd) of metal nanoparticles (MNPs) has been prepared and functionalized with (a) redox-active stalks containing tetrathiafulvalene (TTF) units, (b) [2]pseudorotaxanes formed between these stalks and cyclobis(paraquat-*p*-phenylene) ($CBPQT^{4+}$) rings, and (c) bistable [2]rotaxane molecules where the dumbbell component contains a 1,5-dioxynaphthalene (DNP) unit, as well as a TTF unit, encircled by a $CBPQT^{4+}$ ring. It transpires that the molecules present in (a) and (c) and the supermolecules described in (b) retain their switching characteristics, previously observed in solution, when they are immobilized onto MNPs. Moreover, their oxidation potentials depend on the fraction, χ, of the molecules or supermolecules on the surface of the nanoparticles. A variation in χ affects the oxidation potentials of the TTF units to the extent that switching can be subjected to fine tuning as a result. Specifically, increasing χ results in positive shifts (i) in the oxidation potentials of the TTF unit in (a)−(c) and (ii) the reduction potentials of the $CBPQT^{4+}$ rings in (c). These shifts can be attributed to an increase in the electrostatic potential surrounding the MNPs. Both the magnitude and the direction of these shifts are reproduced by a model, based on the Poisson−Boltzmann equation coupled with charge-regulating boundary conditions. Furthermore, the kinetics of relaxation from the metastable state coconformation (MSCC) to the ground-state coconformation (GSCC) of the bistable [2]rotaxane molecules also depends on χ, as well as on the nanoparticle diameter. Increasing either of these parameters accelerates the rate of relaxation from the MSCC to the GSCC. This rate is a function of (i) the activation energy for the relaxation process associated with the bistable [2]rotaxane molecules in solution and (ii) the electrostatic potential surrounding the MNPs. The electrostatic potential depends on (i) the diameter of the MNPs, (ii) the amount of the bistable [2]rotaxane molecules on the surface of the MNPs, and (iii) the equilibrium distribution of the $CBPQT^{4+}$ rings between the DNP and TTF recognition sites in the GSCC. This electrostatic potential has also been quantified using the Poisson−Boltzmann equation, leading to faithful estimates of the rate constants.

Introduction

Mechanically interlocked molecules[1] (MIMs), such as bistable catenanes and rotaxanes, have been studied intensely in the context of the fundamental understanding of the properties of the mechanical bond,[2] as well as possible applications in nanoelectromechanical systems,[3] mechanized nanoparticles,[4] and molecular electronics.[5] When they are incorporated into electronic devices, the molecules can offer ultrahigh densities of data storage and can provide alternative solutions to the "silicon density challenge". For example, we have reported[6] previously the use of electrochemically switchable, donor−acceptor, bistable [2]catenanes and [2]rotaxanes in molecular-switch tunnel junctions[7] (MSTJs). Recently, bistable [2]rotaxanes have been employed in the construction of a working defect tolerant

(1) (a) Amabilino, D. B.; Stoddart, J. F. *Chem. Rev.* **1995**, *95*, 2725–2828. (b) Breault, G. A.; Hunter, C. A.; Mayers, P. C. *Tetrahedron* **1999**, *55*, 5265–5293. (c) Hubin, T. J.; Busch, D. H. *Coord. Chem. Rev.* **2000**, *200*, 5–52. (d) Collin, J. P.; Dietrich-Buchecker, C.; Gavina, P.; Jimenez-Molero, M. C.; Sauvage, J.-P. *Acc. Chem. Res.* **2001**, *34*, 477–487. (e) Schalley, C. A.; Weilandt, T.; Bruggemann, J.; Vögtle, F. *Top. Curr. Chem.* **2004**, *248*, 141–200. (f) Vickers, M. S.; Beer, P. D. *Chem. Soc. Rev.* **2007**, *36*, 211–225. (g) Stoddart, J. F. *Chem. Soc. Rev.* **2009**, *38*, 1802–1820.

(2) Frisch, H.; Martin, I.; Mark, H. *Monatsh. Chem.* **1953**, *84*, 250–256.

(3) (a) Berna, J.; Leigh, D. A.; Lubomska, M.; Mendoza, S. M.; Perez, E. M.; Rudolf, P.; Teobaldi, G.; Zerbetto, F. *Nat. Mater.* **2005**, *4*, 704–710. (b) Juluri, B. K.; Kumar, A. S.; Liu, Y.; Ye, T.; Yang, Y. W.; Flood, A. H.; Fang, L.; Stoddart, J. F.; Weiss, P. S.; Huang, T. J. *ACS Nano* **2009**, *3*, 291–300.

(4) (a) Saha, S.; Leung, K. C.-F.; Nguyen, T. D.; Stoddart, J. F.; Zink, J. I. *Adv. Funct. Mater.* **2007**, *17*, 685–693. (b) Nguyen, T. D.; Liu, Y.; Saha, S.; Leung, K. C. F.; Stoddart, J. F.; Zink, J. I. *J. Am. Chem. Soc.* **2007**, *129*, 626–634. (c) Coti, K. K.; Belowich, M.; Liong, M.; Ambrogio, M. W.; Lau, Y. A.; Khatib, H. A.; Zink, J. I.; Khashab, N. M.; Stoddart, J. F. *Nanoscale* **2009**, *1*, 16–39.

(5) Dichtel, W. R.; Heath, J. R.; Stoddart, J. F. *Philos. Trans. R. Soc., A* **2007**, *365*, 1607–1625.

(6) (a) Pease, A. R.; Jeppesen, J. O.; Stoddart, J. F.; Luo, Y.; Collier, C. P.; Heath, J. R. *Acc. Chem. Res.* **2001**, *34*, 433–444. (b) Steuerman, D. W.; Tseng, H.-R.; Peters, A. J.; Flood, A. H.; Jeppesen, J. O.; Nielsen, K. A.; Stoddart, J. F.; Heath, J. R. *Angew. Chem., Int. Ed.* **2004**, *43*, 6486–6491.

(7) (a) Collier, C. P.; Jeppesen, J. O.; Luo, Y.; Perkins, J.; Wong, E. W.; Heath, J. R.; Stoddart, J. F. *J. Am. Chem. Soc.* **2001**, *123*, 12632–12641. (b) Diehl, M. R.; Steuerman, D. W.; Tseng, H.-R.; Vignon, S. A.; Star, A.; Celestre, P. C.; Stoddart, J. F.; Heath, J. R. *ChemPhysChem* **2003**, *4*, 1335–1339. (c) DeIonno, E.; Tseng, H.-R.; Harvey, D. D.; Stoddart, J. F.; Heath, J. R. *J. Phys. Chem. B* **2006**, *110*, 7609–7612.

10.1021/ja9102327

160 000 bit molecular memory device[8] with a density of 10^{11} bits per square centimeter.

MIMs which rely upon the preferential binding of a cyclobis(paraquat-*p*-phenylene) ($CBPQT^{4+}$) ring component with a tetrathiafulvalene (TTF) station, relative to a 1,5-dioxynaphthalene (DNP) station, have proven to be efficient molecular switches. In bistable [2]catenanes and [2]rotaxanes based on the TTF and DNP recognition motifs, the $CBPQT^{4+}$ ring exists in equilibrium between the energetically favored TTF station—the ground-state co-conformation, GSCC—and the DNP station—the metastable state co-conformation, MSCC. The oxidation of the TTF unit to its radical cation ($TTF^{\bullet+}$) and then to its dication (TTF^{2+}) gives rise to Coulombic repulsion and causes rapid shuttling or circumrotation involving the $CBPQT^{4+}$ ring, so that it encircles the DNP unit. Conversely, following reduction of the TTF^{2+} dication back to its neutral form, the $CBPQT^{4+}$ ring encircles the DNP station (MSCC), before relaxing back to the GSCC.

The electromechanical switching of both bistable [2]rotaxanes and [2]catenanes has been investigated in a variety of environments,[9,10] including solution, polymer matrices, pendant side chains on polymers,[11] and MSTJs.[12] The relaxation kinetics of these MIMs depends strongly on the environment; for example, increasing solution viscosity significantly slows down the mechanical motion with an observed increase in the activation barrier for the relaxation from the MSCC back to the GSCC. The switching behavior of dithiolane-functionalized bistable [2]rotaxanes has been investigated[13] on flat gold surfaces and also on arrays of gold nanodisks, where the switching of the molecules brought about a significant change in the surface plasmon resonance.

Despite these achievements, the incorporation of MIMs into integrated nanosystems remains challenging. In our most recent research, we have focused on the problem of the conjugation of MIMs with prototypical nanoscale building blocks, such as metal nanoparticles (MNPs). MNPs have been studied[14] intensely because of their unique optical,[15] electronic,[16] catalytic,[17] and mechanical[18] properties. The reason for our motivation to marry MIMs and/or their components with MNPs is that such constructs can yield unique assemblies, useful for the fabrication of nanostructures, in which the chemical and physical properties of both the MIMs and the MNPs are mutually enhanced. In addition, the use of MNPs as "nanoplatforms" for MIMs improves greatly the processability of the latter.[11]

In a recent communication, we reported[19] a methodology for the preparation of MNPs (Au, Pt, Pd), functionalized with dithiolanes terminated in either redox-active MIM components

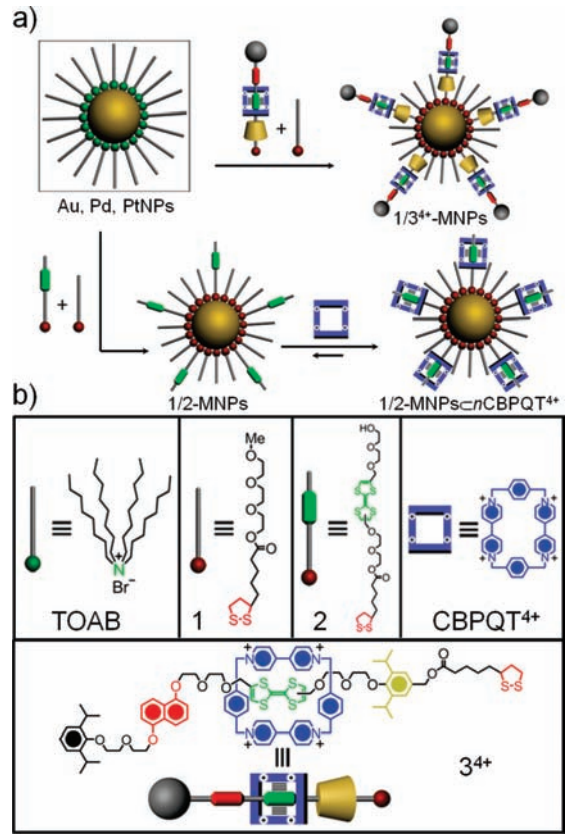

Figure 1. Graphical representation of the functionalization of weakly protected MNPs. (a) TOAB-protected Au, Pt, or Pd MNPs undergo facile ligand exchange when mixed with dithiolanes. Preparation of TTF-functionalized MNPs (**1/2**-MNPs) (bottom left) and the formation of the pseudorotaxane complex **1/2**-MNPs⊂*n*$CBPQT^{4+}$ on the MNP surface (bottom right). Preparation of the bistable [2]rotaxane-functionalized MNPs (**1/3**$^{4+}$-MNPs) (top right). (b) Structural formulas of TOAB, the dithiolane-functionalized triethylene glycol **1**, the TTF derivative **2**, the $CBPQT^{4+}$ ring, and the dithiolane-functionalized bistable [2]rotaxane **3**$^{4+}$. The counterions are PF_6^-.

(8) Green, J. E.; Choi, J. W.; Boukai, A.; Bunimovich, Y.; Johnston-Halperin, E.; DeIonno, E.; Luo, Y.; Sheriff, B. A.; Xu, K.; Shin, Y. S.; Tseng, H.-R.; Stoddart, J. F.; Heath, J. R. *Nature* **2007**, *445*, 414–417.
(9) Flood, A. H.; Peters, A. J.; Vignon, S. A.; Steuerman, D. W.; Tseng, H.-R.; Kang, S.; Heath, J. R.; Stoddart, J. F. *Chem. Eur. J.* **2004**, *10*, 6558–6564.
(10) (a) Huang, T. J.; Tseng, H.-R.; Sha, L.; Lu, W. X.; Brough, B.; Flood, A. H.; Yu, B. D.; Celestre, P. C.; Chang, J. P.; Stoddart, J. F.; Ho, C.-M. *Nano Lett.* **2004**, *4*, 2065–2071. (b) Tseng, H.-R.; Wu, D. M.; Fang, N. X. L.; Zhang, X.; Stoddart, J. F. *ChemPhysChem* **2004**, *5*, 111–116.
(11) Olson, M. A.; Braunschweig, A. B.; Fang, L.; Ikeda, T.; Klajn, R.; Trabolsi, A.; Wesson, P. J.; Benitez, D.; Mirkin, C. A.; Grzybowski, B. A.; Stoddart, J. F. *Angew. Chem., Int. Ed.* **2009**, *48*, 1792–1797.
(12) Choi, J. W.; Flood, A. H.; Steuerman, D. W.; Nygaard, S.; Braunschweig, A. B.; Moonen, N. N. P.; Laursen, B. W.; Luo, Y.; DeIonno, E.; Peters, A. J.; Jeppesen, J. O.; Xu, K.; Stoddart, J. F.; Heath, J. R. *Chem. Eur. J.* **2006**, *12*, 261–279.
(13) Zheng, Y. B.; Yang, Y. W.; Jensen, L.; Fang, L.; Juluri, B. K.; Flood, A. H.; Weiss, P. S.; Stoddart, J. F.; Huang, T. J. *Nano Lett.* **2009**, *9*, 819–825.
(14) Daniel, M. C.; Astruc, D. *Chem. Rev.* **2004**, *104*, 293–346.
(15) (a) Elghanian, R.; Storhoff, J. J.; Mucic, R. C.; Letsinger, R. L.; Mirkin, C. A. *Science* **1997**, *277*, 1078–1081. (b) Storhoff, J. J.; Lazarides, A. A.; Mucic, R. C.; Mirkin, C. A.; Letsinger, R. L.; Schatz, G. C. *J. Am. Chem. Soc.* **2000**, *122*, 4640–4650. (c) Kalsin, A. M.; Pinchuk, A. O.; Smoukov, S. K.; Paszewski, M.; Schatz, G. C.; Grzybowski, B. A. *Nano Lett.* **2006**, *6*, 1896–1903. (d) Kalsin, A. M.; Fialkowski, M.; Paszewski, M.; Smoukov, S. K.; Bishop, K. J. M.; Grzybowski, B. A. *Science* **2006**, *312*, 420–424. (e) Pinchuk, A. O.; Kalsin, A. M.; Kowalczyk, B.; Schatz, G. C.; Grzybowski, B. A. *J. Phys. Chem. C* **2007**, *111*, 11816–11822. (f) Bishop, K. J. M.; Wilmer, C. E.; Soh, S.; Grzybowski, B. A. *Small* **2009**, *5*, 1600–1630.
(16) (a) McConnell, W. P.; Novak, J. P.; Brousseau, L. C.; Fuierer, R. R.; Tenent, R. C.; Feldheim, D. L. *J. Phys. Chem. B* **2000**, *104*, 8925–8930. (b) Nitzan, A.; Ratner, M. A. *Science* **2003**, *300*, 1384–1389. (c) Nakanishi, H.; Bishop, K. J. M.; Kowalczyk, B.; Nitzan, A.; Weiss, E. A.; Tretiakov, K. V.; Apodaca, M. M.; Klajn, R.; Stoddart, J. F.; Grzybowski, B. A. *Nature* **2009**, *460*, 371–375.
(17) (a) Tian, N.; Zhou, Z. Y.; Sun, S. G.; Ding, Y.; Wang, Z. L. *Science* **2007**, *316*, 732–735. (b) Park, J. Y.; Zhang, Y.; Grass, M.; Zhang, T.; Somorjai, G. A. *Nano Lett.* **2008**, *8*, 673–677.
(18) (a) Klajn, R.; Bishop, K. J. M.; Fialkowski, M.; Paszewski, M.; Campbell, C. J.; Gray, T. P.; Grzybowski, B. A. *Science* **2007**, *316*, 261–264. (b) Browne, K. P.; Klajn, R.; Villa, J.; Grzybowski, B. A. *Small* **2009**, *5*, 2656–2658.
(19) Klajn, R.; Fang, L.; Coskun, A.; Olson, M. A.; Wesson, P. J.; Stoddart, J. F.; Grzybowski, B. A. *J. Am. Chem. Soc.* **2009**, *131*, 4233–4235.

such as TTF units or MIMs such as bistable [2]catenanes using weakly protected MNP "precursors".[20] The results of these investigations indicated that surface-attached MIMs retain their switching abilities, and the oxidation potentials of these adsorbed electroactive "switches" depend on their surface fraction on the MNPs.

In the present work, we attempt to understand the physical basis for the switching behavior of nanoparticle-immobilized MIMs and redox-active MIM components. To this end, we prepared Au, Pt, and Pd NPs of varying diameters, functionalized with (i) redox-active stalks containing tetrathiafulvalene (TTF) units, (ii) [2]pseudorotaxanes formed between these stalks and $CBPQT^{4+}$ rings, and (iii) bistable [2]rotaxane molecules (Figure 1) at different surface coverages, χ. The switching behavior of these molecules was investigated using ζ (zeta)-potential and cyclic voltammetry (CV) measurements. The results of these investigations indicate that the redox properties of these molecules and supermolecules can be modulated by the surface composition, χ, as well as the particle diameter, d. Another important conclusion from this work is that the rate of relaxation of the bistable [2]rotaxanes from MSCC to the GSCC accelerates when the values of either χ or d increase. In order to explain these and other experimental findings, we have developed a theoretical model in which the electrostatic potential around the coated MNPs is calculated using the Poisson−Boltzmann equation, coupled to the so-called charge-regulating boundary conditions describing the counterion adsorption equlibria on MNP surfaces. Using only minimal assumptions, this model reproduces the effects of both surface coverage and particle diameter. The calculated values of the electrostatic potential correlate with both the experimentally observed oxidation potentials and the relaxation rates of the immobilized bistable [2]rotaxanes. These results represent, to the best of our knowledge, a pioneering example of the theoretical treatment of the redox properties of molecular-mechanical switching on the surfaces of nanoscopic particles. This theoretical model can be used to guide the rational design of switchable nanoparticles for uses in adaptive materials, nanoelectronic devices, and nanoparticle-based sensors.

Results and Discussion

Design and Synthesis. Insofar as it is a good ligand for gold, dithiolane forms stable bivalent Au−S linkages on either flat gold surfaces or on gold nanoparticles. In order to anchor bistable [2]rotaxanes and redox-active TTF groups on to AuNPs, the dithiolane-terminated TTF **2** and the bistable [2]rotaxane $\mathbf{3}^{4+}$ were designed and synthesized.

The TTF−monodithiolane derivative **2** was prepared (Scheme 1b) in 41% yield, using a carbodiimide-promoted esterification of DEG-TTF[21] **5** with thioctic acid in CH_2Cl_2 at room temperature. Using a similar procedure, esterification of the benzyl alcohol-terminated bistable [2]rotaxane[22] $\mathbf{4}\cdot 4PF_6$ with thioctic acid in MeCN gave (Scheme 1a) the dithiolane-functionalized bistable [2]rotaxane $\mathbf{3}\cdot 4PF_6$ in 53% yield. All of the final products were characterized fully by NMR spectroscopy and mass spectrometry. Correlation NMR spectroscopy ($^1H-^1H$-g-DQF-COSY) at low temperature (233 K) was employed to unravel the ^1H NMR resonances of the $\mathbf{3}\cdot 4PF_6$. See the Supporting Information (SI).

Our initial experiments, aimed at attaching the dithiolanes (DTs) **1**, **2**, and $\mathbf{3}^{4+}$ onto the surface of metal nanoparticles (MNPs), relied upon the use of dodecylamine (DDA)-protected[23] gold MNPs. These attempts, however, failed as a result of the very slow kinetics for the DDA-DT ligand exchange reaction. We found, nonetheless, that the previously described tetraoctylammonium bromide (TOAB)-protected AuNPs (Au·TOAB) undergo[19] the exchange reaction almost instantaneously. Encouraged by these observations, we have extended the Au·TOAB preparation protocol to include palladium and platinum nanoparticles (see the SI) by the reduction of PhMe solutions of tetraoctylammonium tetrahalopalladate, PdX_4^{2-}, and tetrahaloplatinate, PtX_4^{2-}, respectively, with aqueous solutions of sodium borohydride. Au·TOAB, Pd·TOAB, and Pt·TOAB nanoparticles had mean diameters of 4.6 ± 1.2, 2.4 ± 0.6, and 2.7 ± 0.3 nm, respectively, and were readily soluble in PhMe.

With the ultimate goal of studying the effect of the MNPs' size/curvature on switching kinetics of the bistable [2]rotaxane molecules, we synthesized MNPs of different sizes. With small (~2.4 nm PdNPs) and medium-sized (~4.6 nm AuNPs) nanoparticles available (vide supra), a route to larger AuNPs compatible with bistable [2]rotaxane functionalization was desirable. MNP sizes are typically varied by changing the molar ratio of gold to the protecting thiol ligands during the in situ MNP synthesis.[24] It was found, however, that changing the gold/weak TOAB ligand ratio in the ex situ method did not affect the AuNPs' sizes significantly. We therefore pursued another strategy to control the AuNPs' sizes. On the basis of the assumption that a slow addition of the reducing agent would decrease the rate of nucleation relative to the MNP growth

Scheme 1. Synthesis of the Dithiolane-Functionalized (a) Bistable [2]Rotaxane $\mathbf{3}\cdot 4PF_6$ and (b) DEG-TTF **2**

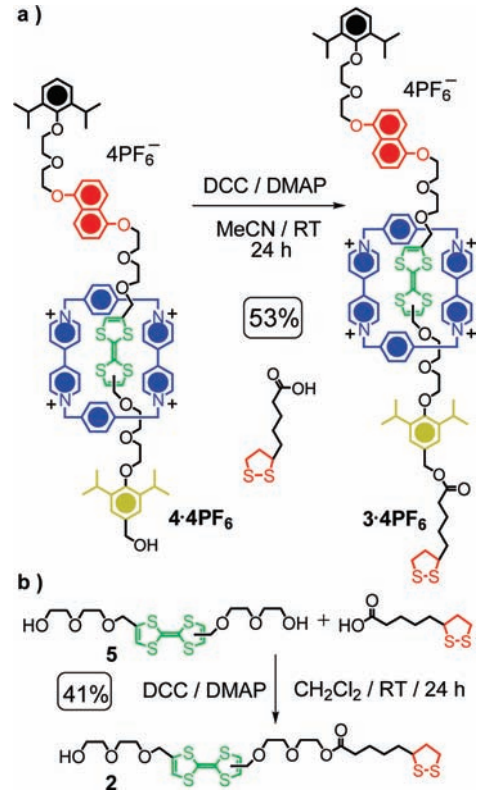

(20) Manna, A.; Chen, P. L.; Akiyama, H.; Wei, T. X.; Tamada, K.; Knoll, W. *Chem. Mater.* **2003**, *15*, 20–28.
(21) Tseng, H.-R.; Vignon, S. A.; Celestre, P. C.; Perkins, J.; Jeppesen, J. O.; Di Fabio, A.; Ballardini, R.; Gandolfi, M. T.; Venturi, M.; Balzani, V.; Stoddart, J. F. *Chem. Eur. J.* **2004**, *10*, 155–172.
(22) Saha, S.; Flood, A. H.; Stoddart, J. F.; Impellizzeri, S.; Silvi, S.; Venturi, M.; Credi, A. *J. Am. Chem. Soc.* **2007**, *129*, 12159–12171.

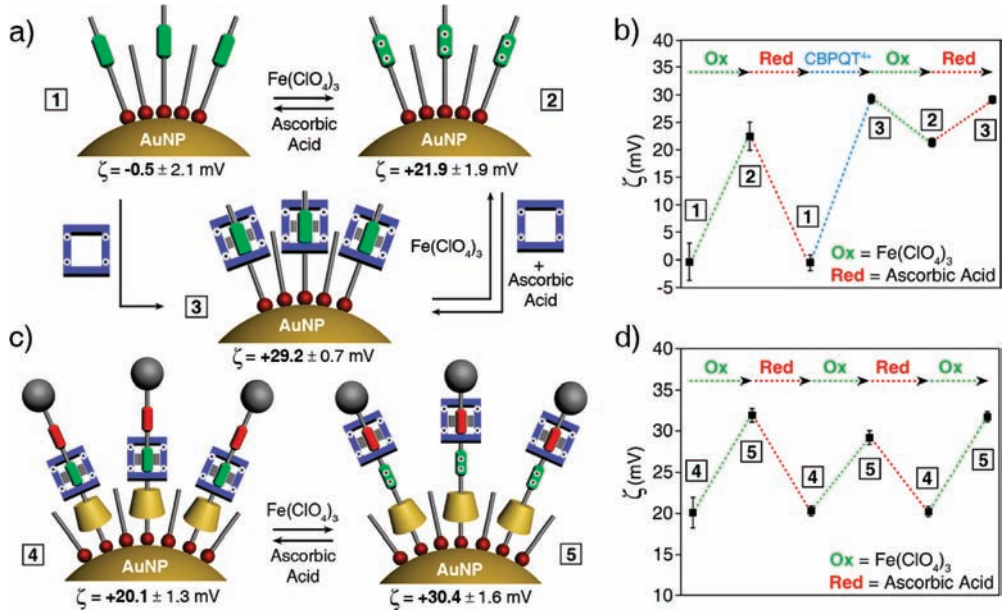

Figure 2. (a) Reversible transformations and ζ-potential values of (1) **1/2**-AuNPs, (2) their oxidized form, **1/2**$^{2+}$-AuNPs, and (3) the pseudorotaxane complex **1/2**-AuNPs⊂*n*CBPQT^{4+}. (b) Changes in ζ-potential for **1/2**-AuNPs as a function of oxidation/reduction (Ox = addition of $Fe(ClO_4)_3$; Red = addition of ascorbic acid) and reversible formation of a pseudorotaxane. (c) Reversible transformations and ζ-potential values for (4) **1/3**$^{4+}$-AuNPs and (5) their oxidized form, **1/3**$^{6+}$-AuNPs. (d) Changes in ζ-potential for **1/3**$^{4+}$-AuNPs (black squares) as a function of reduction/oxidation processes.

process, the $NaBH_4$ solution was added approximately 10 times slower (4 μL s^{-1} vs ~50 μL s^{-1}) than had been reported[19] in the original preparation. The resulting AuNPs indeed had larger diameters (6.6 ± 1.7 nm, compared to 4.6 ± 1.2 nm) and were used to prepare the bistable [2]rotaxane-protected AuNPs by a ligand-exchange reaction.

In order to ensure good solubility of the modified MNPs in polar organic solvents (e.g., MeCN, DMF) suitable for reversible redox chemistry on donor−acceptor bistable [2]rotaxanes, TTF stalks, and their [2]pseudorotaxanes, we prepared MNPs covered with *mixed* self-assembled monolayers (*m*SAMs) comprising the functional ligands **2**, **3**$^{4+}$, and various "inert" background ligands. Ultimately, we found that **1** was the background ligand of choice, simply because it renders **1/2**-MNPs and **1/3**$^{4+}$-MNPs readily soluble[25] in MeOH, MeCN, and DMF.

ζ-Potential Measurements. In order to verify whether and how the harboring of molecular switches on nanoparticles affects their redox switching characteristics, we measured the ζ-potential of **1/2**-AuNPs (χ = 0.25) and **1/3**$^{4+}$-AuNPs (χ = 0.25) (Figure 2a,b) with an average diameter of 4.6 nm, all dissolved in pure DMF ($c_{Au} \approx$ 0.14 mM in terms of gold atoms). In the case of the **1/2**-AuNPs, the ζ-potential had a value close to zero (−0.5 ± 2.1 mV), consistent with the neutral state of the TTF units and an overall neutral surface charge for the MNPs. Oxidation with $Fe(ClO_4)_3$, however, resulted in highly positive values (+21.9 ± 1.9 mV) for the ζ-potential, originating from the oxidized **2**$^{2+}$ moieties on the MNPs' surface. The oxidation process was fully reversible, and addition of an excess of ascorbic acid resulted in the reduction of the **1/2**$^{2+}$-AuNPs back to their neutral state. The ζ-potential measurements could also be used to follow (Figure 2a,b) the formation of the pseudorotaxane **1/2**-AuNPs⊂*n*CBPQT^{4+} on the MNPs. Upon the addition of CBPQT·4PF_6, the ζ-potential increased to +29.2 (±0.7 mV) but reverted to its original value of +21.9 (±1.9 mV) when the **1/2**-AuNPs⊂*n*CBPQT^{4+} were treated with $Fe(ClO_4)_3$. The decrease in the ζ-potential value corresponds to the dethreading processes of the pseudorotaxane, on account of the Coulombic repulsion between the TTF^{2+} dication and the CBPQT^{4+} ring. The **1/3**$^{4+}$-AuNPs had a ζ-potential value of +20.1 (±1.3 mV) before being oxidized with $Fe(ClO_4)_3$. The oxidation of TTF to its dication caused a ca. 51% increase in the ζ-potential (+30.4 ± 1.6 mV) (Figure 2c). This redox cycle could be repeated several times (Figure 2b,d).

Electrochemistry and Theory. Detailed electrochemical investigations have been carried out on MNPs coated with stalks and pseudorotaxanes, as well as on bistable [2]rotaxanes in DMF at various temperatures. The observed trends can be explained by a theoretical model in which the Poisson−Boltzmann equation is used to find a solution for the electrostatic potential around the MNPs, which is subsequently related to the chemical equilibria determining the redox states of the molecular switches. In this section, we discuss first of all the experimental results and their qualitative justification and then develop a more rigorous theoretical description.

(1). Experimental Observations and Qualitative Interpretation.

(a). Stalks and Pseudorotaxanes The switching behavior of MNPs decorated with **2** was investigated by cyclic voltammetry (CV). CV measurements on **2** free in solution, **1/2**-AuNPs, and their pseudorotaxanes—**2**⊂CBPQT^{4+} and **1/2**-AuNPs⊂*n*CBPQT^{4+}, respectively—were carried out in degassed DMF (electrolyte $LiClO_4$, c = 0.05 M, 298 K). As expected, **1/2**-AuNPs (χ = 0.1, 0.5, 1.0) exhibited two reversible one-electron oxidation processes characteristic of the first and second oxidations of the TTF unit. The first oxidation peak (TTF → TTF$^{\bullet+}$) appeared at +608, +657 and +701 mV, and the second oxidation potential (TTF$^{\bullet+}$ → TTF^{2+}) was observed at +910, +958 and +998 mV for χ = 0.1, 0.5, and 1.0, respectively

(23) Jana, N. R.; Peng, X. G. *J. Am. Chem. Soc.* **2003**, *125*, 14280–14281.
(24) (a) Brust, M.; Walker, M.; Bethell, D.; Schiffrin, D. J.; Whyman, R. *J. Chem. Soc., Chem. Commun.* **1994**, 801–802. (b) Yamaguchi, H.; Ikeda, M.; Matsuda, K.; Irie, A. *Bull. Chem. Soc. Jpn.* **2006**, *79*, 1413–1419.
(25) It is important to note that the dilution of **2** and **3**$^{4+}$ with various amounts of **1** was necessary in order to improve the solubility of nanoparticles in polar organic solvents.

(Figure 3a). For all surface coverages, the oxidation potentials of the TTF units on the **1/2**-AuNPs are shifted to more positive values than those—+547 and +789 mV for the first and the second oxidations of the TTF unit, respectively—of **2** in solution. The gradual rise in the oxidation potentials with increasing χ can be attributed to the accumulation of surface charge on the MNPs. In solution, the oxidation of a single TTF unit does not affect the oxidation of additional TTF units. However, if the TTF-containing molecule is adsorbed to the surface of a MNP, then its oxidation will increase the electrostatic potential around that nanoparticle. Consequently, the oxidation of nearby adsorbed TTF stalks will become less energetically favorable, as their oxidation would introduce more positive charge onto the MNP and would further increase the system's electrostatic potential energy. This "negative electrostatic cooperativity" requires a more positive electrostatic potential in order to oxidize adsorbed TTF stalks. These findings demonstrate that the oxidation potentials of redox-active units can be tuned by simply changing their surface coverage on MNPs.

The redox potentials of the TTF unit in **1/2**-AuNPs⊂*n*CBPQT^{4+} pseudorotaxanes are also shifted (Figure 3b) to more positive potentials compared to those of **2**⊂CBPQT^{4+} in solution. CV experiments performed on **2**⊂CBPQT^{4+} in DMF show two oxidation peaks, centered at +595 and +809 mV. The first and second oxidation potentials of the pseudorotaxane (**1/2**-AuNPs⊂*n*CBPQT^{4+}) attached to the surface of AuNPs were observed at +604 and +888 mV at $\chi = 0.1$. In contrast to the TTF stalks, however, these potentials are effectively independent of the surface coverage—that is, no significant shifts were observed for $\chi > 0.1$. These observations are also rationalized using electrostatic arguments—i.e., the formation of adsorbed pseudorotaxanes increases the charge around an MNP monotonically with the amount of threaded CBPQT^{4+}, and it results in the potential around **1/2**-AuNPs⊂*n*CBPQT^{4+} rising with increasing χ. Similarly, after the TTF units have been oxidized and the CBPQT^{4+} rings dethread, the resulting **1/2**$^{\bullet+}$-AuNPs or **1/2**$^{2+}$-AuNPs will also have a surface charge and potential that rise with increasing χ. Thus, the potential difference between the neutral and oxidized states of the tetrathiafulvalene units, corresponding to the additional energy required to oxidize the adsorbed TTF stalks, can remain approximately constant and leads to an effectively constant shift in the oxidation potential as observed for $\chi > 0.1$.

(b). Rotaxanes. CV measurements of **3**·4PF$_6$ and **1/3**$^{4+}$-AuNPs ($\chi = 0.1$, 0.25, 0.50, $d = 4.6 \pm 1.2$ nm) were carried out (Figure 3c) in a degassed DMF solution (electrolyte $LiClO_4$, $c = 0.05$ M) at 298 K. As with **1/2**-AuNPs and **1/2**-AuNPs⊂*n*CBPQT^{4+}, the oxidation potentials for the TTF units in **1/3**$^{4+}$-AuNPs ($d = 4.6$ nm) increases with increasing surface coverage. Unlike the previous cases, however, the oxidation of TTF for $\chi = 0.1$ occurs at a lower potential on the MNPs than it does for free **3**$^{4+}$ in solution. As in the case of the pseudorotaxanes, we attribute the shift in the oxidation potential to the change in potential of the TTF unit in the rotaxane before and after oxidation. In contrast with pseudorotaxanes, however, the CBPQT^{4+} rings present in the rotaxanes do not dethread upon oxidation. Instead, they move from the TTF to the DNP unit and still contribute to the potential around the MNPs, allowing for a positive oxidation potential shift.

Table 1. Experimental and Calculated Kinetic Data for the Relaxation from the MSCC to the GSCC Obtained for **1/3**$^{4+}$-MNPs at Various Surface Coverages and Curvatures[a]

MNP	χ[b]	d[c]	τ (s)	k (s^{-1})	k (s^{-1})[d]	$\Delta G^{\ddagger}$ (kcal·mol^{-1})
PdNP	25	2.4	3.7 ± 0.3	0.27 ± 0.02	0.28	16.2 ± 1.2
AuNP	10	4.6	1.3 ± 0.1	0.76 ± 0.06	0.73	15.6 ± 1.2
AuNP	25	4.6	1.2 ± 0.1	0.83 ± 0.1	0.91	15.5 ± 1.9
AuNP	50	4.6	1.0 ± 0.1	1.0 ± 0.1	0.96	15.4 ± 1.5
AuNP[e]	25	6.6	1.03 ± 0.06	0.98 ± 0.05	0.97	14.6 ± 0.8

[a] Solution data obtained on 0.2 mM samples of MNPs in DMF solution ($LiClO_4$ = 0.05 M used as electrolyte) at 263 K unless otherwise noted. [b] χ = coverage (%). [c] d = diameter (nm). [d] Calculated. [e] Experiment carried out at 251 K.

The relaxation kinetics of the **1/3**$^{4+}$-PdNPs ($\chi = 0.25$), **1/3**$^{4+}$-AuNPs ($\chi = 0.1$, 0.25, 0.50), and larger **1/3**$^{4+}$-AuNPs ($\chi = 0.25$) with diameters, d, of 2.4 ± 0.6, 4.6 ± 1.2, and 6.6 ± 1.7 nm, respectively, were also investigated (Table 1). The TTF unit undergoes sequential and reversible two-electron-oxidation processes, generating cationic species, resulting in a strong Coulombic repulsion between the CBPQT^{4+} ring and the TTF^{2+} dication and so triggering the shuttling of the CBPQT^{4+} ring to the DNP unit in **1/3**$^{4+}$-AuNPs. Reduction of the TTF^{2+} dication back to its neutral state generates the MSCC, which re-equilibrates to the equilibrium mixture of the GSCC and MSCC (9:1). Switching of the GSCC to the MSCC was performed electrochemically and was followed by CV. The kinetics of the

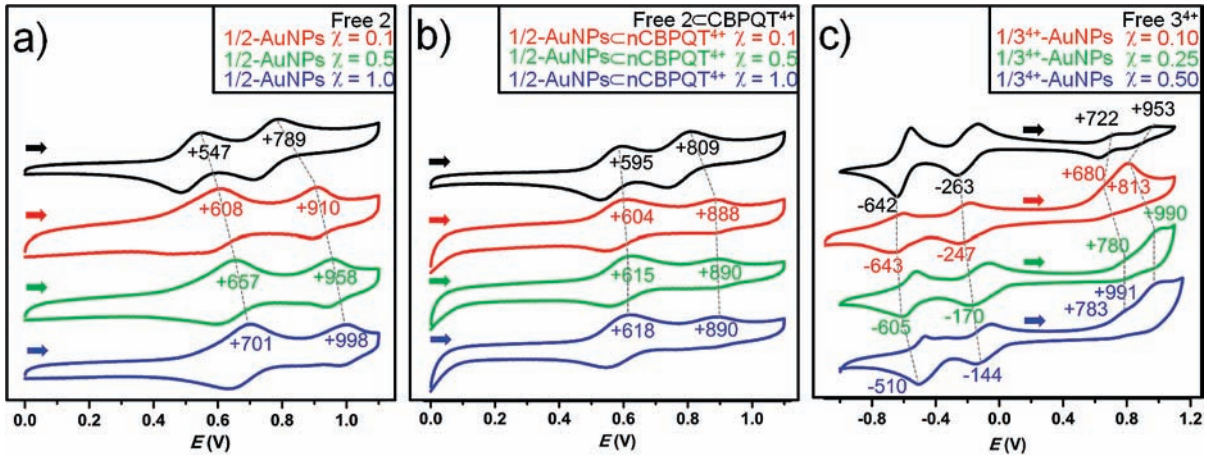

Figure 3. (a) CV of free **2** (black) and **1/2**-AuNPs with surface coverages of **2**: $\chi = 0.1$ (red), 0.5 (green), and 1.0 (blue). (b) CV of free **2**⊂CBPQT^{4+} (black) and **1/2**-AuNPs⊂*n*CBPQT^{4+} with surface coverages of **2**: $\chi = 0.1$ (red), 0.5 (green), and 1.0 (blue). (c) CV of free **3**$^{4+}$ (black) in solution and **1/3**$^{4+}$-AuNPs with surface coverages of **3**$^{4+}$: $\chi = 0.1$ (red), 0.25 (green), and 0.5 (blue). Solution data were obtained on 0.2 mM samples of AuNPs in DMF solution (0.05 M $LiClO_4$ used as electrolyte) at 298 K.

relaxation of the MSCC back to the GSCC were quantified by changing the scan rate (50 to 1000 mV s^{-1}) in CV experiments and fitting a first-order decay model to the population ratios of the MSCC and the relaxation times. While at slow scan rates the $CBPQT^{4+}$ ring has sufficient time to relax back to the GSCC between the first and the second CV cycles, much faster scan rates reveal the MSCC wherein the $CBPQT^{4+}$ ring has yet to relax to the GSCC. The ratio of the two translational isomers can be calculated by the integration of the first and second oxidation peaks of two successive CV scans. The first oxidation peak (N_{DNP}) of the second scan arises from the MSCC in which the $CBPQT^{4+}$ ring encircles the DNP unit. The second peak area (N_{TTF}) corresponds to the thermodynamically more stable isomer (GSCC), while the sum of the first and second oxidation peak areas ($N_{DNP} + N_{TTF} = N_{total}$) corresponds to the total number of $\mathbf{3}^{4+}$ molecules on the MNP surface. Our initial experiments at ambient temperatures have revealed that the kinetics of the relaxation from the MSCC back to the GSCC were too fast to be measured on the CV time scale. In order to slow down the relaxation process, the CV experiments were carried out at or below 263 K. The lifetime of the MSCC at 263 K was found to be 1.3(±0.1) s for $\mathbf{1/3}^{4+}$-AuNPs ($\chi = 0.1$, $d = 4.6 \pm 1.2$ nm) with a $\Delta G^{\ddagger}$ value of 15.6(±1.2). Increasing the surface coverage very slightly decreases the free energy of activation ($\chi = 0.25$, $\Delta G^{\ddagger} = 15.5 \pm 1.9$ kcal mol^{-1} and $\chi = 0.50$, $\Delta G^{\ddagger} = 15.4 \pm 1.5$ kcal mol^{-1}). We also prepared mixed self-assembled monolayers incorporating **1** and $\mathbf{3}^{4+}$ on surfaces with a range of curvatures—$\mathbf{1/3}^{4+}$-PdNPs ($d = 2.4 \pm 0.6$ nm) and $\mathbf{1/3}^{4+}$-AuNPs ($d = 4.6 \pm 1.2$ and 6.6 ± 1.7 nm) at a constant surface coverage of $\chi = 0.25$. The rate of relaxation of $\mathbf{3}^{4+}$ from the MSCC to the GSCC on the surfaces of PdNPs was found to be 0.27(±0.02) s^{-1}, translating into a free energy of activation of 16.2(±1.2) kcal mol^{-1}. Decreasing the particle's curvature caused a concomitant increase in the rate of relaxation. We observed a rate of relaxation of 0.80(±0.1) s^{-1} ($\Delta G^{\ddagger} =$ 15.5(±1.2) kcal mol^{-1} at 263 K) and 0.98(±0.05) s^{-1} ($\Delta G^{\ddagger} =$ 14.6(±0.8) kcal mol^{-1} at 251 K) for the $\mathbf{1/3}^{4+}$-AuNPs with average core diameters of 4.6 and 6.6 nm, respectively. Note that the relaxation rate of the adsorbed rotaxanes is slower than for those in solution, yet faster than in polymer matrices and SAMs on flat gold surfaces.[9]

The changes in the relaxation rate of adsorbed rotaxanes can be related to the potential surrounding the particles. In the CV experiments the measured decay time is related to the rate of relaxation from the MSCC to the GSCC and also to the equilibrium distribution of $CBPQT^{4+}$ rings in the GSCC.[12] The adsorption of rotaxanes onto the MNP surfaces increases the potential of the TTF unit relative to the DNP unit, causing more of the $CBPQT^{4+}$ rings to encircle the DNP units in the GSCC and also increasing the activation energy for the MSCC to the GSCC relaxation process. Since the potential difference between the TTF and DNP units is a function of both the MNP diameter and χ, the relaxation rates also depend on both χ and MNP diameter. See Table 1.

(2). Theoretical Interpretation. The qualitative arguments developed in Section 1 can be formalized within the framework of a theoretical model which relates observed shifts in the oxidation potential, E, of adsorbed redox-active molecules to the oxidation-induced changes in the electrostatic potential, Φ, surrounding the MNPs. Two observations are relevant here: (i) that the oxidation of switches, X, adsorbed on MNP surfaces causes Φ around the particle to increase and (ii) that the more oxidized species already present on the surface, the more difficult it is to oxidize more of these groups and introduce additional charge onto the particle. On the basis of these premises, the oxidation potential of adsorbed X should be related to Φ. To a first approximation, it can be assumed that this relationship is linear, such that the shift in the oxidation potential of the switches upon MNP immobilization, i.e., from the solution value $E(X,0)$ to the on-particle value $E(X,\chi)$, is equal to the change in the electrostatic potential at the surface of a functionalized MNP. Mathematically

$$E(X,\chi) - E(X,0) = \Phi(X^{ox},\chi,a) - \Phi(X^{red},\chi,a) \qquad (1)$$

where, as before, χ is the surface fraction of molecules of type X on the nanoparticle, and a is equal to the radius of the MNP plus monolayer. Note that if the reduced molecules are also uncharged (e.g., as in the TTF stalks), $\Phi(X^{red},\chi,a) = 0$; if, however, they are charged (e.g., as in the pseudorotaxanes or rotaxanes), $\Phi(X^{red},\chi,a) \neq 0$. Also, one way to understand eq 1 is to relate the reduction and electrostatic potentials to the free energy differences describing the system, as illustrated in Figure 4a.

The electrostatic potential surrounding the MNP can be calculated using the Poisson−Boltzmann (PB) equation. Using the nondimensional potential $\psi = e\Phi/k_BT$ (e is the charge of an electron, k_B is Boltzmann's constant, and T is the temperature), this equation can be written as $\nabla^2\psi = \kappa^2 \sinh(\psi)$, where κ^{-1} is the Debye screening length. For spherically symmetrical MNPs, the PB equation becomes $r^{-2}(\partial)/(\partial r)(r^2(\partial\psi)/(\partial r)) = \kappa^2 \sinh(\psi)$. The boundary conditions are that the potential infinitely far from each particle—in dilute solution—tends to zero and the

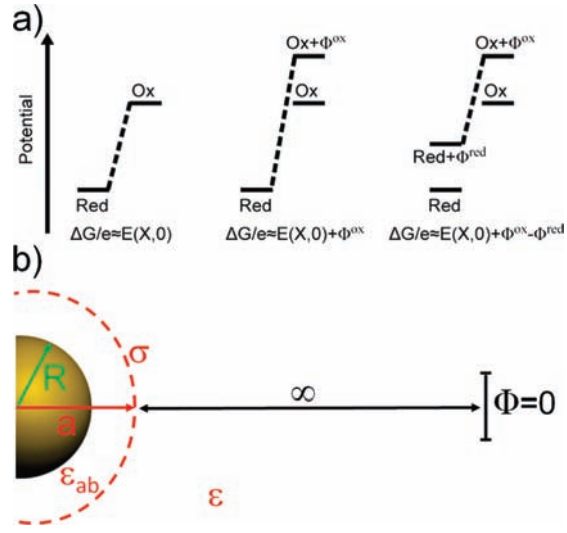

Figure 4. (a) Schematic energy diagram for the oxidation of a redox-active molecule X immobilized on MNPs. In solution (left), there is a characteristic free energy change, $e\,E(X,0)$, associated with the molecule's oxidation. If the molecule is initially adsorbed onto an electrically neutral particle (middle), its oxidation produces a potential, Φ^{ox}, around that particle. The free energy of oxidation for an adsorbed particle is then equal to the characteristic free energy change plus the energy required to raise the potential of the oxidized molecule from zero (if it were in solution) to Φ^{ox}. Similarly, if the molecule is adsorbed on an initially charged surface with potential Φ^{red}, after oxidation, its potential must be adjusted from Φ^{red} to Φ^{ox}. If Φ^{ox} is greater than Φ^{red}, the free energy of oxidation will be increased by $e(\Phi^{ox} - \Phi^{red})$. (b) Scheme showing half of a spherical MNP with radius R. Upon oxidation, adsorbed TTF stalks create a shell of charge around this MNP at radius a with a surface charge density σ. Inside this shell, the dielectric constant is approximated as ε_{ab}, while outside the shell the dielectric constant of the solution is ε. Infinitely far from the particle, the potential Φ is zero.

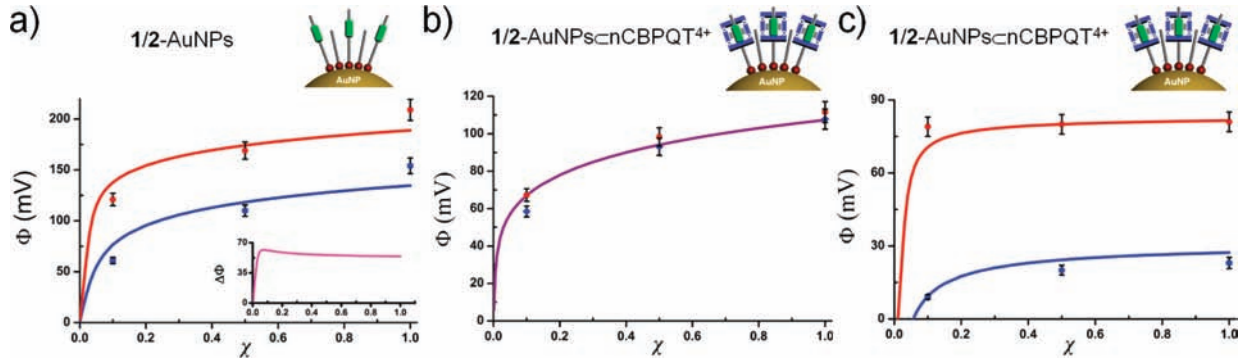

Figure 5. (a) Calculated potentials $\Phi(\mathbf{2}^{ox\_1}, \chi)$ (blue line) and $\Phi(\mathbf{2}^{ox\_2}, \chi)$ (red line) for **1/2**-AuNPs along with the measured first (blue markers) and the second (red markers) oxidation potential shifts of **2** adsorbed on AuNPs as a function of the surface coverage, χ. The inset shows the difference $\Phi(\mathbf{2}^{ox\_2}, \chi)$-$\Phi(\mathbf{2}^{ox\_1}, \chi)$. (b) Close agreement of the the potential of **1/2**-AuNPs⊂CBPQT^{4+} from the first oxidation (red markers) and second oxidation (blue markers) of **1/2**-AuNPs⊂CBPQT^{4+}, and the predicted value of $\Phi(\mathbf{2}^{red}, \chi)$ (purple line). (c) Very close agreement of the difference between $\Phi(\mathbf{2}^{ox\_i},\chi)$- $\Phi(\mathbf{2}^{red},\chi)$ for $i = 1$ (red line) and $i = 2$ (blue line) with the experimentally observed oxidation shifts for the first (red markers) and second (blue markers) oxidations of **1/2**-AuNPs⊂CBPQT^{4+}.

only immobile charges are located on a spherical surface (of some radius $r = a$) within the SAM (Figure 4b) so that $(\partial\psi)/(\partial r)|_{r=a} = -(e\sigma(X^{ox},\chi,\psi))/(k_B T\varepsilon_0\varepsilon)$ (a so-called "charge-regulating" boundary condition[26]), where σ is the surface charge density, ε_0 is the permittivity of free space, and ε is the dielectric constant of the solution (here, $\varepsilon = 38.25$ for DMF[27]). For each charged ligand that is attached to the surface of a MNP, some counterions from solution—denoted as Z—associate with that charged molecule and effectively decrease the total amount of charge surrounding the MNP (the counterions are either ClO_4^- from the electrolyte or PF_6^- initially bound to the CBPQT^{4+} rings). At the same time, the equilibria describing counterion association/adsorption depend on the electrostatic potential around the MNP; hence, in the "charge-regulating" boundary condition,[26] σ also depends on ψ. In other words, the equations describing the electrostatics of the MNP systems are coupled through the boundary conditions. One way to solve them is to use a procedure in which an estimated solution ψ is adjusted iteratively until the system of equations reaches convergence. For further mathematical details, see the SI. With these general considerations in mind, we consider the specific types of molecules used in this investigation.

(a). TTF Stalks. The oxidation potential for both the first and the second oxidations of **2** adsorbed on the **1/2** AuNPs increases with increasing χ (see Figure 5a). In this system, the fully reduced form of **2** is neutral, so that $\psi(\mathbf{2}^{red},\chi,a) = 0$. Note that there are two oxidation peaks in the CV curves. These peaks correspond to the formation of $\mathbf{2}^{\bullet+}$ radical cations—henceforth denoted ox_1—and $\mathbf{2}^{2+}$ dications (ox_2). Substituting into eq 1, we find that the shifts in the oxidation potential are equal to $\psi(\mathbf{2}^{ox\_i},\chi,a)$, where $i = 1, 2$. The effective surface charge density, σ, is then calculated by (i) multiplying the number of dithiolane-TTF ligands adsorbed onto one MNP, $\pi d^2\chi/A_{DT}$—where $A_{DT} = 42.8$ Å^2 is the area occupied by one dithiolane ligand and is roughly twice the area required for one thiol to bind onto AuNP[28]—by the average charge of one ligand, $e\gamma$ and (ii) dividing by the area of the shell of charge at $r = a$. This manipulation gives $\sigma = d^2 e\gamma\chi/4a^2 A_{DT}$, where the value of γ can be determined from a set of equations describing the equilibria of counterion adsorption. These equations are of the form

$$\frac{[X^{ox\_i}\, yZ]}{[X^{ox\_i}\,(y-1)Z][Z]} = K(X^{ox\_i})\exp(\psi) \qquad (2)$$

where $1 \le y \le i$ ($i = 1, 2$, determined by the oxidation state of the TTF unit) is the number of adsorbed counterions Z, $K(X^{ox\_i})$ is the equilibrium constant for the association of the counterions in the absence of electrostatic potential, and the exponential term accounts for the shift in the equilibrium arising from the finite potential around the particle at a given χ. Assuming that the concentration of counterions is constant—ca. 50 mM, in large excess relative to ~0.3 mM X—the set of equilibrium in eq 2 can be solved to give

$$\gamma(X^{ox\_i}, a) = \frac{\sum_{n=1}^{i} n(K(X^{ox\_i})[Z]\exp(\psi))^{-n}}{\sum_{n=0}^{i}(K(X^{ox\_i})[Z]\exp(\psi))^{-n}} \qquad (3)$$

Using the experimental values of the metal core diameter $d = 4.6$ nm, an estimated monolayer thickness of 1.2 nm (so that $a = 3.5$ nm), and $T = 298$ K leaves only the binding constants $K(\mathbf{2}^{ox\_1})$ and $K(\mathbf{2}^{ox\_2})$ as the unknown parameters ultimately required to calculate ψ. In order to obtain these two constants, the sum of the squared error between the calculated values of ψ—using "estimated" pairs of $K(\mathbf{2}^{ox\_1})$ and $K(\mathbf{2}^{ox\_2})$—and the experimental data is minimized iteratively until convergence using a Newtonian search algorithm. This procedure yields $K(\mathbf{2}^{ox\_1}) = 1.19$ M^{-1} and $K(\mathbf{2}^{ox\_2}) = 0.121$ M^{-1}. Also see section 4 in the SI. These binding constants are then used, in conjunction with the charge-regulating boundary condition and the PB equation, to compute the theoretical values of $\psi(\mathbf{2}^{ox\_1},\chi,a)$ and $\psi(\mathbf{2}^{ox\_2},\chi,a)$ for $\chi = 0$ to 1. Figure 5a shows that the predictions of $\psi(\mathbf{2}^{ox\_1},\chi,a)$ and $\psi(\mathbf{2}^{ox\_2},\chi,a)$ from the theoretical model are in excellent agreement with the experiments and do reproduce the increase in the oxidation potentials with increasing χ. Qualitatively, this result captures the "cross-talk" between the immobilized redox-active molecules, whereby the oxidation potential of each molecule within the SAM is influenced by its neighbors.

(26) Bishop, K. J. M.; Grzybowski, B. A. *ChemPhysChem* **2007**, *8*, 2171–2176.
(27) *CRC Handbook of Chemistry and Physics*; Lide, D. R.:, Ed.; CRC Press: New York, 2005.
(28) Leff, D. V.; Ohara, P. C.; Heath, J. R.; Gelbart, W. M. *J. Phys. Chem.* **1995**, *99*, 7036–7041.

(b). Pseudorotaxanes. When MNPs decorated with X^{red} = TTF⊂CBPQT^{4+} complexes—i.e., **1/2**-AuNPs⊂*n*CBPQT^{4+}—are oxidized, the CBPQT^{4+} rings dethread, leaving AuNPs coated with oxidized **2** as either $X^{ox\_1} = \mathbf{2}^{\bullet+}$ or $X^{ox\_2} = \mathbf{2}^{2+}$. In contrast with the simple **1/2**-AuNPs described earlier where the shifts in the oxidation potentials and the electrostatic potentials both increase with χ (Figure 5a), the experimentally observed magnitude of the shifts $E(X,\chi) - E(X,0)$ for the first and second oxidations of **1/2**-AuNPs⊂*n*CBPQT^{4+} remain approximately constant for $\chi > 0.10$ (Figure 5c).

This result can be explained by the fact that adsorption of the charged CBPQT^{4+} rings onto **1/2**-AuNPs—i.e., onto fully reduced **2**—causes the "reference" electrostatic potential $\psi(X^{red},\chi,a)$ of the **1/2**-AuNPs⊂*n*CBPQT^{4+} to increase with increasing χ. Consequently, *both* $\psi(X^{ox},\chi,a)$ and $\psi(X^{red},\chi,a)$ increase with χ, but their calculated difference remains (Figures 4a (right) and 5b) approximately constant for $\chi > 0.10$.

In order to calculate $\psi(X^{red},\chi,a)$, it is necessary to determine the surface charge density, which depends on both the equilibration during threading of CBPQT^{4+} rings on surface-immobilized **2** stalks and the adsorption equilibrium of counterions onto the formed TTF⊂CBPQT^{4+} pseudorotaxanes. The first of these equilibria is determined from

$$\frac{[X^{red}]}{[\mathbf{2}][\text{CBPQT}^{4+}]} = K_{PS}\exp(-4\psi) \tag{4}$$

where the binding constant for pseudorotaxane formation, $K_{PS} = 4.16 \times 10^5$ M^{-1}, was taken from the literature[12] and the exponential term accounts for the additional energy necessary to "raise" CBPQT^{4+} rings from a potential of 0 in solution to a potential of ψ when they are adsorbed onto the nanoparticle. Concurrently, the association of counterions with MNP-bound **2**⊂CBPQT^{4+} pseudorotaxanes is described by a set of adsorption equilibria, analogous to eq 2, with the difference that there are up to four counterions per one pseudorotaxane. Hence, there are four equilibria of the form

$$\frac{[X^{red}\ yZ]}{[X^{red}\ (y-1)Z][Z]} = K(X^{red})\exp(\psi) \tag{5}$$

where $y = 1$ to 4 and the equilibria are coupled to eq 4. After some algebra, two quantities can be obtained: θ, which is the fraction of TTF stalks forming pseudorotaxanes with CBPQT^{4+} rings, and γ, which gives the average charge of these pseudorotaxanes surrounded by counterions. For the detailed calculations, see section 4 in the SI.

As in the case of TTF stalks (section 2a), the effective surface charge density is given by $\sigma = ed^2\chi\theta\gamma/4a^2A_{DT}$, which is used to calculate the electrostatic potential employing the Poisson–Boltzmann equation. The experimental parameters describing this system are $d = 4.6$ nm, $a = 3.5$ nm, and $T = 298$ K as before, with the initial concentrations of the adsorbed **2** on the MNPs, $[\mathbf{2}]_0 = 0.014$, 0.070, and 0.14 mM for $\chi = 0.1$, 0.5, and 1.0, respectively, while the CBPQT^{4+} concentration in solution is $[\text{CBPQT}^{4+}]_0 = 1.4$ mM. The only unknown parameter is the binding constant of counterions Z to **2**⊂CBPQT^{4+}, $K(\mathbf{2}\subset\text{CBPQT}^{4+})$, which is found—using Newton's method to fit to experimental oxidation potentials—to be $K(\mathbf{2}\subset\text{CBPQT}^{4+}) = 5.01$ M^{-1}.

The second electrostatic potential which needs to be calculated, $\Phi(X^{ox\_i},\chi,a)$, corresponds to the situation when the CBPQT^{4+} rings dethread from the oxidized TTF stalks. Under these conditions, the MNPs become identical with those treated in the section 2a and eqs 2 and 3 can be applied. Figure 5c demonstrates that the difference of the electrostatic potentials thus calculated, $\psi(X^{ox\_i},\chi,a) - \psi(X^{red},\chi,a)$, reproduces faithfully the experimentally observed shifts in the oxidation potentials for all values of χ studied.

(c). Rotaxanes. In contrast to the stalks or pseudorotaxanes, where the charges are distributed over one spherical shell ($r = a$), the charges in the rotaxane counterpart can reside at either the TTF or DNP units, which for the MNP systems correspond (Figure 6a) to two "shells" of charge at, respectively, $r = a$ (ca. 1.2 nm from the MNP surface) and $r = b$—ca. 2 nm from the MNP surface. An important consequence is that, in order to calculate electrostatic potentials, it is necessary to determine the distribution of charges between these two shells. In order to do this calculation, we need to consider the kinetics of the relaxation of the CBPQT^{4+} rings from the DNP to the TTF unit of the rotaxane: i.e., the relaxation between the metastable state coconformation, MSCC, and the ground state coconformation, GSCC.

Specifically, the experimentally measured time constant τ_{relax} for the MSCC to GSCC relaxation can be related to the intrinsic relaxation rate constant k_f by $\tau_{relax} = (1 - x)/k_f$, where x is the fraction of the CBPQT^{4+} rings encircling the DNP units at equilibrium.[12] In the MNP/rotaxane systems, the value of x is influenced by the electrostatic potential difference between the TTF and DNP units. Hence, the equilibrium equations can be written as

$$\frac{[\text{DNP}\subset\text{CBPQT}^{4+}]}{[\text{TTF}\subset\text{CBPQT}^{4+}]} = \exp\left(\frac{-\Delta G}{RT}\right)\exp(-4(\psi(b) - \psi(a))) \tag{6}$$

where $\Delta G = 3$ kcal mol^{-1} is the Gibbs free energy difference between the two states[29] and the exponential term accounts for the energy required to move a CBPQT^{4+} ring from the potential, $\psi(a)$, at the TTF unit to the potential, $\psi(b)$, at the DNP unit. In order to calculate the fractions of DNP⊂CBPQT^{4+} and TTF⊂CBPQT^{4+}, it is also necessary to account for the association of counterions with the CBPQT^{4+} rings, as described in eq 6. We assume that the binding constants of counterions Z to the CBPQT^{4+} rings at either unit—TTF or DNP—are the same, i.e., $K(\text{DNP}\subset\text{CBPQT}^{4+}) = K(\text{TTF}\subset\text{CBPQT}^{4+}) = K(\text{CBPQT}^{4+})$, which leads to the following expression for x:

$$x = \frac{\rho(b)\exp\left(\frac{-\Delta G}{RT}\right)\exp(-4(\psi(b) - \psi(a)))}{\rho(a) + \rho(b)\exp\left(\frac{-\Delta G}{RT}\right)\exp(-4(\psi(b) - \psi(a)))} \tag{7}$$

where $\rho(r) = \sum_{q=0}^{4}(K(\text{CBPQT}^{4+})[Z]\exp(\psi(r)))^q$ quantifies the binding of counterions to the CBPQT^{4+} rings. The second parameter necessary to estimate τ_{relax} is the forward reaction rate, k_f, which we estimate using the Eyring equation:

$$k_f = \frac{k_B T}{h}\exp\left(-\left(\frac{\Delta G^{\ddagger}}{RT} + \alpha 4(\psi(a) - \psi(b))\right)\right) \tag{8}$$

where the first term in the exponent is the activation free energy with no external field, the second term adjusts the activation

(29) Kang, S. S.; Vignon, S. A.; Tseng, H.-R.; Stoddart, J. F. *Chem. Eur. J.* **2004**, *10*, 2555–2564.

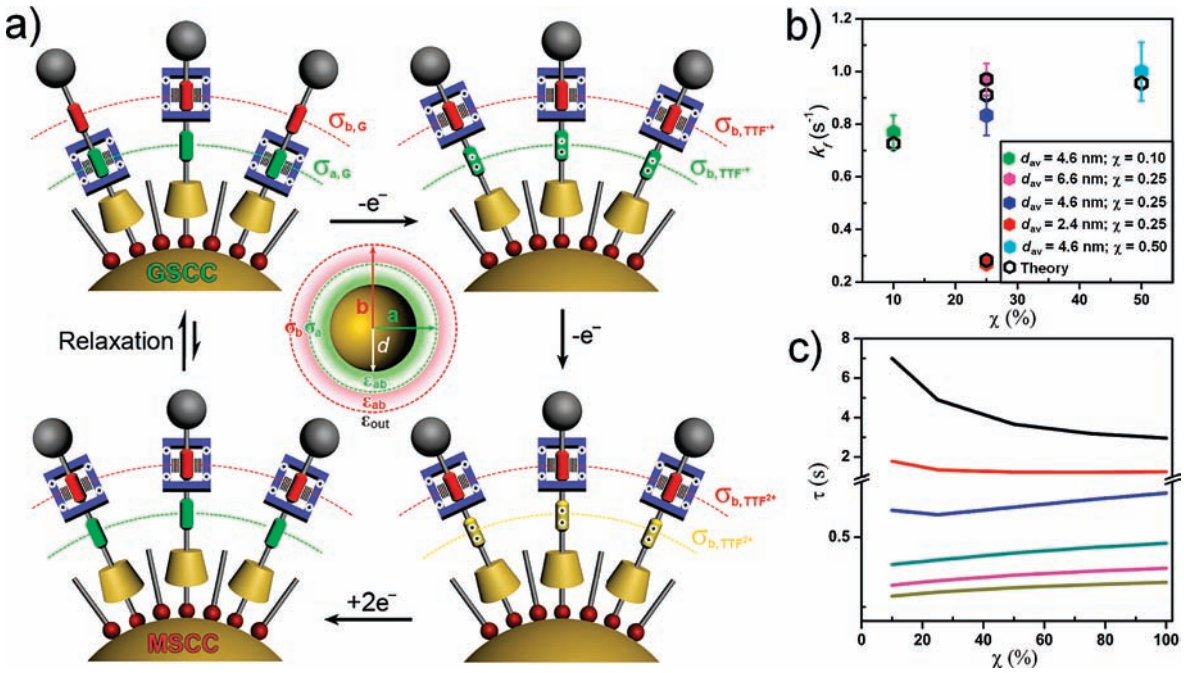

Figure 6. (a) Scheme illustrating the location of the $CBPQT^{4+}$ rings and charge densities around MNPs for $\mathbf{3}^{4+}$ in its (clockwise from upper left) GSCC, first oxidation, second oxidation, and MSCC states. (b) Experimental (filled markers) and theoretical (empty black hexagons) relaxation rates for the MSCC to GSCC transition. (c) Theoretical values of the relaxation time for different diameter MNPs. The diameters are (top to bottom) 2, 4, 8, 12, 16, and 20 nm.

energy by the change in potential of a $CBPQT^{4+}$ ring as it moves through a potential field, and the parameter $0 < \alpha < 1$ represents the fraction of the electrostatic potential energy difference between the two TTF and DNP units that influences the activation energy.[30]

In order to calculate the potentials required to estimate τ_{relax}, we use the PB equation with charge-regulating boundary conditions to obtain ψ for the GSCC. In the beginning, we calculated the surface charge densities at the TTF unit, $\sigma(a)$, and the DNP unit, $\sigma(b)$, from the value of x and the number of charges per $CBPQT^{4+}$ ring at location r, $\gamma(CBPQT^{4+},r)$. The estimation of σ then follows a procedure similar to that used for the TTF stalks. Specifically, for $\sigma(a)$, we multiply the number of adsorbed rotaxanes $\pi d^2\chi/A_{DT}$ by the fraction $1 - x$ of rotaxanes with the $CBPQT^{4+}$ ring encircling the TTF unit and the number of charges per $CBPQT^{4+}$ ring, $e\gamma(CBPQT^{4+},a)$ and then divide by the area of the shell of charge at $r = a$. Similarly, for $\sigma(b)$ the number of rotaxanes is multiplied by the number of charges per $CBPQT^{4+}$ ring at $r = b$ and by the fraction (x) of rotaxanes with the $CBPQT^{4+}$ ring encircling the DNP unit and is divided by the area of the shell of charge with radius $r = b$:

$$\sigma(a) = \frac{ed^2\chi(1-x)}{4\varepsilon_0 A_{DT} a^2}\gamma(CBPQT^{4+}, a)$$
$$\sigma(b) = \frac{ed^2\chi x}{4\varepsilon_0 A_{DT} b^2}\gamma(CBPQT^{4+}, b) \quad (9)$$

These surface charge densities are then used in the charge regulating boundary conditions at $r = a$ and $r = b$, as well as zero surface charge at $r = d/2$ and $\psi = 0$ at $r = \infty$ as:

$$\varepsilon_{ab}\frac{\partial\psi}{\partial r}\bigg|_{a^+} - \varepsilon_{ab}\frac{\partial\psi}{\partial r}\bigg|_{a^-} = -\frac{e\sigma(a)}{k_B T\varepsilon_0}$$
$$\varepsilon\frac{\partial\psi}{\partial r}\bigg|_{b^+} - \varepsilon_{ab}\frac{\partial\psi}{\partial r}\bigg|_{b^-} = -\frac{e\sigma(b)}{k_B T\varepsilon_0} \quad (10)$$
$$\frac{\partial\psi}{\partial r}\bigg|_{d/2} = 0$$

where the dielectric constant of the monolayer is estimated to be the same as that for diethylene glycol,[27] so that $\varepsilon_{ab} = 31.82$. The experimental MNP diameters, χ, and T are then the inputs in the calculation of ψ—using the PB equation and eqs 6−10—and $K(CBPQT^{4+})$ is calculated from $K(CBPQT^{4+}) = \exp(-\Delta G_{CBPQT^{4+}}/RT)$. We then minimize the sum of squared error between τ_{relax} values as measured experimentally and as calculated using the PB equation, $\tau_{relax} = (1 - x)/k_f$, and eqs 6−10 by varying α, $\Delta G_{CBPQT^{4+}}$, $\Delta H^{\ddagger}$, and $\Delta S^{\ddagger}$. The best-fit parameters found in this way were $\Delta G_{CBPQT^{4+}} = 0.18$ kcal mol^{-1}, $\alpha = 0.370$, $\Delta H^{\ddagger} = 6.60$ kcal mol^{-1}, and $\Delta S^{\ddagger} = -40.7$ cal mol^{-1} K^{-1}. The calculated values of $\Delta H^{\ddagger}$ and $\Delta S^{\ddagger}$ are close to values previously reported for rotaxanes and can be used to estimate $\Delta G^{\ddagger}_{298\,K} = 18.7$ kcal mol^{-1}, which is also in good agreement

(30) As the $CBPQT^{4+}$ ring moves from the DNP to the TTF station, it passes through a high-energy transition state between the two stations. At this location, the ring is also at a higher electrostatic potential than when it is on the DNP station; this electrostatic energy difference effectively raises the activation energy of the process relative to its solution value. In order to estimate the magnitude of this change, we assume that the activation energy of the DNP-to-TTF relaxation process is increased by a portion of the maximum electrostatic energy difference between the two stations observed in this process, a situation which occurs when the $CBPQT^{4+}$ rings are in their equilibrium distribution. The magnitude of this activation energy increase is determined by varying the parameter $0 < \alpha < 1$ to produce the best fit with experimental data. We use α to estimate this energy difference because we do not know empirically where the transition state is, and so we cannot calculate the potential directly at its location.

with previous findings.[12] The values of $k_f = 1/\tau_{relax}$ calculated with these parameters are in very good agreement with the experimental results, as shown in Figure 6b—for MNPs with a given χ, the lifetime of the MSCC decreases with increasing MNP diameter (Figure 6c). This observation can be explained qualitatively by considering the distance between the charged areas of the adsorbed molecules. At constant χ, the distance between charged molecules decreases with increasing diameter, d; thus, the Coulombic respulsions between molecules will increase, thereby destabilizing the MSCC as the MNP diameter increases. Similarly, for smaller MNPs, the lifetime decreases with increasing χ, a situation which also causes an increase in the Coulombic repulsions and MSCC destabilization.

Next, we extended the model to estimate the shifts in the oxidation potentials. Specifically, the potentials of both the TTF and DNP units change as a function of the oxidation state of the TTF and also as a function of the rotaxane coverage on the MNP surface. In order to relate the calculated potentials to the observed oxidation potential shifts, we assume that the scaled energy associated with oxidation potential shift,

$$e(E(X,\chi) - E(X,0))/k_BT$$

is equal to the sum of the energy required to raise the oxidized TTF unit from $\psi(X^{red},\chi,a)$ to $\psi(X^{ox\_i},\chi,a)$ plus the energy required to raise the $CBPQT^{4+}$ rings from an average potential of $x\psi(X^{red},\chi,b) + (1 - x)\psi(X^{red},\chi,a)$ to $\psi(X^{ox\_i},\chi,b)$. These considerations can be summarized as

$$\frac{e}{k_BT}(E(X,\chi) - E(X,0)) = i(\psi(X^{ox\_i},\chi,a) - \psi(X^{red},\chi,a)) + 4(\psi(X^{ox\_i},\chi,b) - x\psi(X^{red},\chi,b) - (1 - x)\psi(X^{red},\chi,a)) \quad (11)$$

where $i = 1, 2$ is the oxidation state of the TTF unit. This calculation is similar to the case of the pseudorotaxanes in that the potential change of the TTF units contributes to the oxidation potential shift. In addition, because the $CBPQT^{4+}$ rings are permanently attached to the MNP and increase the potential of the TTF units both before and after oxidation, the energetic change upon rotaxane switching also affects the shifts in the oxidation potentials of the TTF units.

In order to calculate the potential of the TTF units before oxidation, the PB equation is solved with the charge densities and boundary conditions defined by eqs 9 and 10. After oxidation, the $CBPQT^{4+}$ rings all shift to the DNP stations, so that the charge densities are given as

$$\sigma(a) = \frac{ed^2\chi}{4\varepsilon_0 A_{DT} a^2}\gamma(TTF^{ox\_i}, a)$$
$$\sigma(b) = \frac{ed^2\chi}{4\varepsilon_0 A_{DT} b^2}\gamma(CBPQT^{4+}, b) \quad (12)$$

where $i = 1, 2$ denotes the oxidation state of the TTF units and γ is calculated as described in eq 3. The shift in the oxidation potential is then estimated using eq 11.

The potentials were calculated using the same set of parameters as for the rotaxane kinetics with $d = 4.6$ nm, $a = 3.5$ nm, $b = 4.3$ nm, $T = 298$ K, $\varepsilon = 38.25$, and $\varepsilon_{ab} = 31.82$, which left only the binding constants of Z to $CBPQT^{4+}$, TTF^{ox_1}, and TTF^{ox_2}, $K(CBPQT^{4+})$, $K(TTF^{ox\_1})$, and $K(TTF^{ox\_2})$, respectively, as unknown parameters to fit to the experimental data. Least-squares fitting of these parameters to the data at $\chi = 0.25$ and $\chi = 0.5$ gave $K(CBPQT^{4+}) = 0.051\ M^{-1}$, $K(TTF^{ox\_1}) = 0.019\ M^{-1}$, and $K(TTF^{ox\_2}) = 0.077\ M^{-1}$. Using these parameters, the predictions are that, for sufficiently high surface coverage of rotaxanes, the oxidation potential of TTF increases with increasing χ. This very simple model, however, does not predict the *negative* oxidation potential shift at low surface coverages (Figure 7).

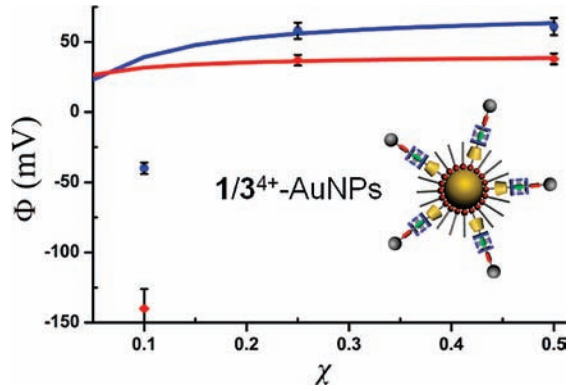

Figure 7. Experimental (markers) and calculated (lines) potentials at the TTF station for the first (blue) and second (red) oxidations of TTF in bistable [2]rotaxanes on MNPs—$\Phi(\mathbf{3}^{ox\_i},\chi) - \Phi(\mathbf{3},\chi)$ for $i = 1, 2$ for $\mathbf{1/3}^{4+}$-AuNPs. The model does not reproduce experimental data for low values of surface coverage, where the charges from rotaxanes may not be evenly distributed over the surface of the MNP.

(d). Limitations of the Model. While the model we developed can reproduce the oxidation potential shifts and changes in relaxation kinetics for most of the MNP systems studied, it becomes less accurate as χ approaches zero. This limitation manifests itself most prominently in the case of MNP-immobilized rotaxanes, where the theory does not account (Figure 7) for the negative shift in oxidation potential for $\chi = 0.1$. Here, two assumptions may be questioned. First, we assume that, for both stalks and rotaxanes, the fraction of redox-active molecules adsorbed onto the MNPs is identical with their fraction in solution. This assumption appears to be valid for the uncharged dithiolanes, as the uncharged functionalized dithiolanes can bind to MNP surfaces at approximately the same rate as the background thiolane ligands.[19] This assumption, however, is not valid for the bistable [2]rotaxanes, since each adsorbing rotaxane contains a mechanically bound charged $CBPQT^{4+}$ ring—when more than one rotaxane is adsorbed onto the surface of an MNP, there will be an energetically unfavorable Coulombic interaction between the rotaxane molecules. This interaction will shift the equilibrium distribution of rotaxanes on the surface of an MNP and will result in χ values smaller than the fraction of the rotaxane molecules in solution. Second, when χ is small, there are very few charged ligands adsorbed on an MNP—for $\chi = 0.1$, there are ca. 15 ligands—and so the assumption that the charge is homogeneously distributed on a spherical shell surrounding the MNP becomes less reliable. Under such conditions, the electrostatic potential surrounding the MNP is no longer spherically symmetric and, in principle, the exact distribution of the redox ligands should be taken into account when calculating the potential.

Conclusions

Weakly protected Au, Pt, and Pd NPs have all been functionalized successfully with (i) redox-active stalks containing TTF units, (ii) pseudorotaxanes formed between these stalks and $CBPQT^{4+}$ rings, and (iii) bistable [2]rotaxane molecules. These molecular and supramolecular entities retain their switch-

ing properties at the MNP−solvent interface. It has been shown that, by varying the surface coverages and/or the MNP diameters, both the redox properties and the rates of relaxation of these switches can be controlled. The relaxation kinetics of switchable bistable [2]rotaxanes on the surfaces of MNPs—from the MSCC to the GSCC—have been shown to be faster than those in which the bistable [2]rotaxanes are incorporated into a polymer matrix or onto flat gold surfaces, but they remain slower than for the same switches in solution. These findings have been explained using a model based on the Poisson−Boltzmann equation. To the best of our knowledge, this work presents the only theoretical treatment of molecular-mechanical switching on nanoparticle surfaces to be carried out to date. Importantly, the model we have developed can be applied to any system of adsorbed molecules where an external "stimulus" changes the surface charge density. In essence, this model can be used to guide the rational design of switchable nanoparticles for uses in adaptive materials, nanoelectronic devices, and nanodelivery systems. Finally, these findings indicate[12] that the switching characteristics of mechanically interlocked molecules, such as bistable rotaxanes, take place by a universal mechanism, irrespective of environment.

Acknowledgment. This research was supported by the Non-equilibrium Energy Research Center (NERC), which is an Energy Frontier Research Center funded by the U.S. Department of Energy, Office of Science, Office of Basic Energy Sciences, under Award Number DE-SC0000989.

Supporting Information Available: Text and figures giving experimental details, spectroscopic characterization data, and additional theory. This material is available free of charge via the Internet at http://pubs.acs.org.

JA9102327